HHS Public Access

Author manuscript

Cancer Res. Author manuscript; available in PMC 2022 January 20.

Published in final edited form as:

Cancer Res. 2021 June 15; 81(12): 3295–3308. doi:10.1158/0008-5472.CAN-20-3564.

Inhibition of Granulocytic Myeloid-Derived Suppressor Cells Overcomes Resistance to Immune Checkpoint Inhibition in LKB1-deficient Non-Small Cell Lung Cancer

Rui Li[1,*], **Ramin Salehi-Rad**[1,2,*], **William Crosson**[3], **Milica Momcilovic**[1], **Raymond J. Lim**[3], **Stephanie L. Ong**[1], **Zi Ling Huang**[1], **Tianhao Zhang**[3], **Jensen Abascal**[1], **Camelia Dumitras**[1], **Zhe Jing**[1], **Stacy J. Park**[1], **Kostyantyn Krysan**[1], **David B. Shackelford**[1,3], **Linh M. Tran**[1], **Bin Liu**[1,**], **Steven M. Dubinett**[1,2,3,4,5,**]

[1]Department of Medicine, Division of Pulmonary and Critical Care, David Geffen School of Medicine at UCLA, 10833 Le Conte Avenue, 43-229 CHS, Los Angeles, CA 90095-1690, USA

[2]Department of Medicine, VA Greater Los Angeles Healthcare System, 11301 Wilshire Boulevard, Los Angeles, CA 90073, USA

[3]Department of Molecular and Medical Pharmacology, David Geffen School of Medicine at UCLA, 650 Charles E. Young Drive South, 23-120 CHS, Box 951735, Los Angeles, CA 90095-1735, USA

[4]Department of Pathology and Laboratory Medicine, David Geffen School of Medicine at UCLA, 757 Westwood Plaza, Los Angeles, CA 90095, USA

[5]Jonsson Comprehensive Cancer Center, UCLA, 8-684 Factor Building, Box 951781, Los Angeles, CA 90095-1781, USA

Abstract

LKB1 inactivating mutations are commonly observed in patients with KRAS-mutant non-small cell lung cancer (NSCLC). While treatment of NSCLC with immune checkpoint inhibitors (ICI) has resulted in improved overall survival in a subset of patients, studies have revealed that co-occurring KRAS/LKB1 mutations drive primary resistance to ICIs in NSCLC. Effective therapeutic options that overcome ICI resistance in LKB1-mutant NSCLC are limited. Here we report that loss of LKB1 results in increased secretion of the C-X-C motif (CXC) chemokines with an NH2-terminal Glu-Leu-Arg (ELR) motif in premalignant and cancerous cells, as well as in genetically engineered murine models (GEMM) of NSCLC. Heightened levels of ELR+ CXC chemokines in LKB1-deficient murine models of NSCLC positively correlated with increased abundance of granulocytic myeloid-derived suppressor cells (G-MDSC) locally within the tumor

**Corresponding authors: Bin Liu and Steven M. Dubinett. David Geffen School of Medicine at UCLA, 10833 Le Conte Avenue, 43-229 CHS, Los Angeles, CA 90095-1690, USA. Phone: 310-267-2725; bliu@mednet.ucla.edu; sdubinett@mednet.ucla.edu.
*Contributed equally to this work.

Author's contributions: R.L., S.M.D. conceived the original concept. R.L., R.S.R, B.L. planned the experiments. R.L, R.S.R, M.M., W.C., R.J.L, C.D., J.A., S.J.P., S.L.O., Z.L.H, Z.J., T.Z. carried out the experiments. R.L. and R.S.R. wrote the manuscript with support from D.B.S., K.K., B.L., S.M.D. B.L. and S.M.D supervised the research. All authors provided critical feedback and contributed to the research analysis.

Conflicts of Interest: Steven M. Dubinett is an advisory board member for EarlyDiagnostics Inc., T-Cure Bioscience Inc., LungLife AI Inc., and Johnson and Johnson Lung Cancer Initiative.

microenvironment and systemically in peripheral blood and spleen. Depletion of G-MDSCs with antibody or functional inhibition via all-trans-retinoic acid (ATRA) led to enhanced anti-tumor T cell responses and sensitized LKB1-deficent murine tumors to PD-1 blockade. Combination therapy with anti-PD-1 and ATRA improved local and systemic T cell proliferation and generated tumor-specific immunity. Our findings implicate ELR+ CXC chemokine-mediated enrichment of G-MDSCs as a potential mediator of immunosuppression in LKB1-deficient NSCLC and provide a rationale for utilizing ATRA in combination with anti-PD-1 therapy in patients with LKB1-deficient NSCLC refractory to ICIs.

Keywords

NSCLC; KRAS; LKB1; ELR+ CXC chemokines; MDSCs; immunotherapy

Introduction

The development of ICIs has transformed the therapeutic landscape of NSCLC. Currently, anti-PD-1/PD-L1 treatment is the first-line therapy for advanced-stage NSCLC patients, either as monotherapy or in combination with chemotherapy(1–3). Although anti-PD-1 therapy has led to improved survival in a subset of NSCLC patients(2–4), the majority of patients do not respond and many develop resistance(5). Studies reveal that responses to ICIs are associated with preexisting $CD8^+$ T cells(6) and high baseline PD-L1 expression in the TME(7). Tumor mutational burden (TMB)(8) and clonal neoantigen burden(9) have also been associated with improved responses to ICIs. In contrast, factors that mediate resistance to PD-1/PD-L1 blockade remain poorly understood.

LKB1 inactivating mutations are found in 20% of patients with NSCLC and one-third of *KRAS*-mutant NSCLCs(10). LKB1 is an upstream activator of the energy-sensing kinase AMPK, which inhibits mTOR signaling(11). Therefore, loss of LKB1 confers a direct proliferative advantage to cancer cells. Studies revealed that loss of LKB1 in NSCLC is associated with a distinct immune profile characterized by diminished T cell infiltration, low or absent PD-L1 expression, and abundance of neutrophils in the TME(12–14). A recent landmark report demonstrated that inactivating mutations of *LKB1* in NSCLC are the major genetic driver of primary resistance to anti-PD-1 therapy(13).

Herein, we report that loss of LKB1 induces heightened production of the ELR+ CXC chemokines in *in vitro* and *in vivo* lung cancer models. The abundance of the ELR+ CXC chemokines in *Kras*-mutant NSCLCs with LKB1 deficiency is associated with an enrichment of G-MDSCs locally within the TME and systemically in peripheral blood and spleen of tumor-bearing mice. Depletion of G-MDSCs by anti-Gr-1 or functional blockade of G-MDSCs with ATRA reverses immune suppression and sensitizes LKB1-deficient tumors to PD-1 blockade. ATRA therapy represents a potential therapeutic strategy to overcome resistance to anti-PD-1 immunotherapy in *LKB1*-mutant NSCLC.

Materials and Methods

Cell lines and cell culture

Immortalized human bronchial epithelial cell (HBEC) lines and HBEC-cancer cell pairs were generously provided by John D. Minna, M.D. at UT Southwestern(15) and cultured, as previously described(16). Stable HBEC cell lines containing either a control beta-galactosidase (βgal) or a mutant $KRAS^{V12}$ (KRAS) were generated, as previously described(17). NSCLC cell lines H441, H1838, H1793, H1568, H322, A549, and H838, as well as the prostate cancer cell line, MyC-CaP, were purchased from ATCC and cultured in complete media [RPMI1640 (Corning) with 10% fetal bovine serum (FBS)]. Murine NSCLC lines established from $Kras^{G12D}Tp53^{-/-}Luc$ (KP), $Kras^{G12D}Tp53^{+/-}LKB1^{-/-}Luc$ (KPL) tumors were previously described(18). Cells were maintained at 37^0C in a humidified incubator with 5% CO_2, and utilized before 5 passages. Cell lines were genotyped by STR profiling (DNA IQ System and Powerplex 1.2 system, Promega) and confirmed to be free of Mycoplasma (MycoAlert, Lonza).

Gene knockdown by RNA interference

Stable isogenic cell lines were established via transduction with retro- or lenti-virus and selected with puromycin (EMD chemicals) for 10 to 14 days, as previously described(19). Short-hairpin RNA (shRNA) lenti-viral constructs containing a non-silencing (NS) sequence or a sequence against LKB1 (CATCTACACTCAGGACTTCAC) (shLKB1) were purchased from Sigma. Retro-viral constructs carrying empty vector (V), wild type LKB1 (WT-LKB1) or kinase dead LKB1 (KD-LKB1) were purchased from Addgene. For transient LKB1 silencing, cells were transfected with small interfering RNA (siRNA) as previously described(19). SiRNAs against LKB1 (siLKB1) or scramble control (sictrl) were pooled siRNAs purchased from Dharmacon GE healthcare.

Luminex-based multiplex assay

Luminescent-based cytokine screening was performed with a customized panel of forty-five human cytokines/growth factors (Bio-Rad). Fresh medium was added to HBEC cells at 20% confluence and cells were incubated for 72 hours. Supernatants were collected and centrifuged to remove floating cells. Samples were analyzed in triplicate. Results were normalized to 1×10^6 cells from matched samples.

Protein extraction and Western Blot

Western Blots were performed, as previously described(19). Anti-LKB1 antibody was purchased from Cell Signaling Technology (Clone 27D10). Anti-GAPDH antibody was from Advanced Immunochemical Inc (Clone 6C5).

Enzyme-linked immunosorbent assay (ELISA)

Cells at 20% confluence were incubated for 72 hours in 1 ml of fresh media. CXCL1/CXCL8 concentrations in the supernatant were quantified with DuoSet ELISA (R&D Systems). Murine serum was prepared by resting 0.5 ml of whole blood at room temperature for 30 minutes followed by centrifugation at 2000g for 10 min. Bronchoalveolar lavage

(BAL) supernatant was harvested after samples were centrifuged at 2000g for 10 min. Supernatants of cells transfected with siLKB1 or sictrl were collected 72 hours post-transfection. Bicinchoninic acid (BCA) assay was performed on lysates from adherent cells to determine the protein concentration. ELISA results were normalized by protein concentration.

RNA extraction and quantitative real time polymerase chain reaction (q-PCR)

Total RNA was isolated using Quick-RNA MiniPrep (Zymo), and cDNA was synthesized with High-Capacity RNA-to-cDNA Kit (Life Technologies). Expression levels of chemokine genes were examined by q-PCR using gene-specific primers (Supplemental Table) and normalized to *GAPDH*(19).

Bioinformatics

RNA-seq and genotyping of cancer cell lines were downloaded from Broad Institute Cancer Cell Line Encyclopedia (CCLE. https://portals.broadinstitute.org/ccle, date: 12–24-2019). NSCLC cells were hierarchically classified into high and low clusters based on chemokine expression. Each chemokine was normalized to the geometric mean of its expression in all cells. The occurrence of *KRAS* and *LKB1* double mutations in each cluster was compared using Fisher's exact test. Custom codes are available at https://github.com/Tian-hao/CCLE

Studies with GEMMs

Studies with GEMMs utilized Lox-Stop-Lox *Kras*^{G12D};*Lkb1*$^{Lox/Lox}$;Rosa26-Lox-Stop-Lox-*Luc* (KL), Lox-Stop-Lox *Kras*^{G12D};*Tp53*$^{Lox/Lox}$;Rosa26-Lox-Stop-Lox-*Luc* (KP), and Lox-Stop-Lox *Kras*^{G12D};Rosa26-Lox-Stop-Lox-*Luc* (K) mice on an FVB background(20). Lung tumors were induced by intranasal administration of 2.5×10^6 plaque forming units (PFUs) of Adeno-Cre (Gene Transfer Vector Core, University of Iowa) as previously described(21). KL and KP mice were euthanized 10–12 weeks after tumor induction, and K mice 25–28 weeks post tumor induction. Lung tumors were dissected and subjected to downstream assays. For early-stage BAL studies, mice were euthanized 4 weeks after administration of 2.5×10^7 PFUs of Adeno-Cre. Mice were housed in pathogen-free facilities at UCLA. All experimental procedures were approved by the UCLA Animal Research Committee.

Studies in syngeneic and immunodeficient mice

FVB and NOD.Cg-*Prkdc*^{scid} *Il2rg*^{tm1Wjl}/SzJ (NSG) mice were purchased from Charles River Laboratories. Tumor cells were implanted in 7–9-week-old mice subcutaneously. To obtain murine blood, tumor-bearing mice were subjected to retro-orbital bleeding on day 9 and day 14 and cardiac puncture at euthanasia on day 15. For therapeutic studies, mice bearing ~50mm^3 tumors were randomized and treated with 200 μg of anti-PD-1 antibody (BioXcell, Clone RMP1–14), 200 μg of anti-Gr-1 antibody (BioXcell, Clone BE0075) or isotype control via intra-peritoneal (IP) injections 2–3 times per week for 5 doses. In ATRA studies, 200 μg of ATRA (dissolved in 10% DMSO, 10% Tween 80, and 80% PBS) was administered daily, starting on day 5. Bioluminescence images were obtained by IVIS Spectrum imager 10 min after IP injection of D-luciferin (150mg/kg). In secondary tumor challenge studies, mice were euthanized when tumor volume reached 12000 mm^3.

Immunophenotyping by flow cytometry

Single-cell suspension from murine spleens and tumors were prepared as previously described(18). To obtain circulating leukocytes, murine blood collected in Ethylenediaminetetraacetic acid (EDTA) was treated with red blood cell lysis buffer (BioLegend). Surface staining and intracellular staining for FOXP3 and Ki-67 were performed as previously described(18). IFNγ and TNFα production was evaluated by intracellular staining after *in vitro* stimulation with Cell Stimulation Cocktail (eBioscience) for 4 hours, utilizing the intracellular fixation and permeabilization buffer set (eBioscience). Data acquisition was performed on Attune NxT cytometer (ThermoFisher), and data analyzed by FlowJo software (TreeStar). Reagents and antibodies utilized are detailed in the Supplemental Table.

In vitro proliferation assay

Cells were plated in culture media with or without ATRA in 96-well plates (1000 tumor cells or 3000 G-MDSCs per well) in triplicates. Proliferation was measured using ATPlite 1step Luminescence Assay Kit (Perkin Elmer) every 24 hours up to 120 hours.

T cell suppression assay

Single-cell suspension of 6 tumors from each group (ATRA-treated and untreated) were pooled 10 days after tumor inoculation. Live G-MDSCs ($MHCII^{lo}CD11b^{+}Ly6C^{lo}Ly6G^{+}$) were sorted with BD FACSAria II (BD Biosciences). Splenic $CD3^{+}$ T cells were isolated from naïve mice utilizing magnetic negative selection (BioLegend). T cells were labeled with CellTrace Violet (Invitrogen) and plated in a 96-well U-bottom plate (1×10^{5} cells per well) in complete media. Flow-sorted G-MDSCs from control or ATRA-treated tumor-bearing mice were added at varying proportions to T cells and incubated overnight. The following day, T cells were treated with 1×10^{5} αCD3/αCD28 Dynabeads (ThermoFisher) and 10ng/mL murine IL2 (PeproTech). T cell proliferation was evaluated by flow cytometry 4 days after stimulation. For *in vitro* treatment, sorted G-MDSCs from control mice were pre-treated with 2μM ATRA for 24 hours. Culture media was replaced with fresh media to remove ATRA prior to co-culturing with T cells.

Statistical analysis

Experiments were performed at least three times, unless otherwise indicated. Results from one representative experiment are shown. Statistical analyses were performed in Prism 9 (GraphPad) unless otherwise noted. Statistical significance was determined using an unpaired, parametric *t*-test with 95% confidence interval. Results are reported as mean ± SEM, unless indicated. Tumor growth curve was analyzed using two-way ANOVA with Tukey post-test for time-associated comparison among multiple groups. Statistical significance is reported as the following: * $P<0.05$; **, $P< 0.01$; ***, $P<0.001$; ****, $P< 0.0001$.

Results

LKB1-loss induces the expression of ELR+ CXC chemokines in HBECs

To understand the effect of LKB1-loss on the production of cytokines in lung cancers, we first utilized immortalized HBECs which lack other cancer phenotypes and retain the ability to differentiate into normal bronchial epithelium(15). Given that *LKB1* mutations frequently co-occur with *KRAS* mutations in human NSCLC, we stably knocked down *LKB1* by shRNA in HBEC3 cells containing either a control βgal or a mutant KRAS vector (Fig. 1A). Screening a panel of commonly dysregulated cytokines and growth factors in human cancer revealed that LKB1-loss in HBEC3 cells increased the production of many of these factors (36/45 in βgal and 35/45 in KRAS). Notably, LKB1 knockdown resulted in upregulation of the ELR+ CXC chemokines Gro-α (CXCL1) and IL-8 (CXCL8) in both βgal and KRAS HBEC3 cells (Fig. 1B). These results were validated by ELISA (Fig 1C).

To evaluate whether this upregulation was broadly applicable, we transiently silenced LKB1 via siRNA in four additional parental HBEC lines (H2, H3, H4, and H7) (Supplementary Fig. S1A) and found increased CXCL1 and CXCL8 expression at both RNA and protein levels (Fig. 1D). Expression of other ELR+ CXC genes, including *CXCL2*, *CXCL3*, and *CXCL5*, was also increased in all HBECs with LKB1 knockdown compared to controls, except for *CXCL5*, which was not detected in H3 and H4 (Fig. 1E). Transient LKB1 knockdown also resulted in elevated CXCL8 secretion in KRAS-transduced HBEC cell lines (H4-KRAS and H7-KRAS) (Fig. 1F). We examined CXCL8 production in two sets of paired HBECs and cancer cells (HCCs) derived from the same patient, HBEC4058/HCC4058 and HBEC4087/HCC4087 (Fig. 1G). Cancer cells produced higher amounts of CXCL8 at baseline compared to their HBEC counterparts, and LKB1-loss resulted in significantly increased CXCL8 secretion (Fig. 1G). These data demonstrate that loss of LKB1 induces ELR+ CXC chemokine expression in HBECs and cancer cells.

LKB1 regulates ELR+ CXC chemokines in human NSCLC cell lines

We stably knocked down LKB1 in the *KRAS*-mutant H441 NSCLC cell line and observed elevated expression of *CXCL2*, *CXCL3*, *CXCL5*, and *CXCL8* at the transcriptional level and increased CXCL8 protein production by ELISA (Fig. 2A and Supplementary Fig. S1B). Similarly, transient knockdown of LKB1 in *KRAS* wild-type NSCLC cell lines, H1838 and H1793, led to a two-to-nine-fold increase in the expression of ELR+ CXC chemokines, as revealed by q-PCR, except for *CXCL8* expression which did not change in H1793 (Fig. 2B and Supplementary Fig. S1C). This observation may be due to the complex transcriptional regulation of *CXCL8* which can be governed by promoter methylation(22).

Next, we re-expressed WT-LKB1 or KD-LKB1 in A549 cells, which harbor an intrinsic *LKB1* mutation that results in the deletion of the LKB1 protein (Fig. 2C). Re-introduction of WT-LKB1 in A549 cells decreased the expression of *CXCL1*, *CXCL2*, *CXCL3*, *CXCL5*, and *CXCL8* (Fig. 2C). A decrease in CXCL1 and CXCL8 protein production was demonstrated by ELISA (Fig. 2D). In contrast, the expression of ELR+ chemokines was not altered in A549 cells that expressed KD-LKB1 except for a statistically significant minor reduction in *CXCL8*. These findings indicate that the kinase activity of LKB1 is

required for the suppression of ELR+ CXC chemokines. Similar results were observed with re-introduction of WT-LKB1 and KD-LKB1 in another LKB1-deficient NSCLC cell line H838, except for the expression of *CXCL5* which was not altered by LKB1 status (Fig. 2E and Supplementary Fig. S1D). Methylation of the *CXCL5* gene has also been reported as a regulatory mechanism(23). To assess if LKB1-loss results in selective induction of ELR+ CXC chemokines, the expression of *CXCL9* and *CXCL10* was assessed in A549 and H838 cells. *CXCL10* expression was not altered by introduction of WT-LKB1 in H838 cells (Supplementary Fig S1E), while the expression of *CXCL9* was below detection. *CXCL9* and *CXCL10* expression was undetectable in isogenic A549 cell lines. Collectively, these findings establish LKB1 as a negative regulator of ELR+ CXC chemokine transcription in NSCLC cell lines, which requires the kinase activity of LKB1.

An unsupervised clustering analysis of chemokine expression in 138 NSCLC cell lines from CCLE(24) revealed that 16 of 18 cell lines with co-occurring *KRAS/LKB1* mutations were stratified into Cluster 1 (C1) with high ELR+ CXC chemokine expression (p=0.00394) (Fig. 2F). However, *LKB1* mutation alone did not lead to a significant C1 distribution of the cell lines (p=1). This is likely due to the fact that multiple genomic alterations can upregulate the expression of ELR+ CXC chemokines in cancer cells(25–29). We observed that cancer cells consistently produce higher amounts of CXCL8 compared to their HBEC counterparts (Fig. 1G). These results suggest that *KRAS* and *LKB1* co-mutation may serve as a genetic biomarker that predicts high expression of ELR+ CXC chemokines in human NSCLC.

Heightened levels of ELR+ CXC chemokines in preclinical LKB1-deficient NSCLC tumors are associated with a G-MDSC-enriched microenvironment

In vivo expression of ELR+ CXC chemokines was examined utilizing GEMMs of LKB1-deficient NSCLC. Increased expression of ELR+ CXC chemokines was observed in lung tumors from KL mice compared to KP or K mice (Fig. 3A). Given that ELR+ CXC chemokines mediate similar biological functions through common receptors (CXCR1 and CXCR2), an overall score that incorporated the expression of ELR+ CXC chemokines was calculated to reflect their cumulative abundance. The mean overall chemokine score in KL tumors was more than four log-fold higher compared to that in KP or K tumors (Fig. 3B). No difference was observed between KP and K tumors. We also evaluated the protein level of CXCL1 as a representative ELR+ CXC chemokine in the BAL fluid of KL and KP mice and noted a significantly higher level in KL mice (Fig. 3C and Supplementary Fig. S2A). Similarly, gene expression analysis of ELR+ CXC chemokines in multiple murine NSCLC cell lines generated from GEMMs (Supplementary Fig. S2B) revealed an increased expression and a higher overall chemokine score in KPL cell lines compared to that in KP cell lines (Fig. 3D).

Given that ELR+ CXC chemokines play a critical role in the trafficking of G-MDSCs from bone marrow to inflammatory sites(30,31), we assessed whether LKB1-loss in GEMM tumors results in an enrichment of G-MDSC in the TME. A significantly higher percentage of G-MDSCs was observed within the immune population of the TME in KL tumors than KP tumors of comparable size (58.5% vs. 7.6%, $p < 0.0001$) (Fig. 3E and Supplementary Fig. S2C). The content of monocytic-MDSCs (M-MDSCs) was less than 1% of the total

immune cells in KL and KP tumors (Supplementary Fig. S2D). To further investigate the association between the level of ELR+ CXC chemokines and G-MDSC tumor-infiltration, three KPL and two KP cell lines that possessed graded levels of ELR+ CXC chemokines (Fig. 3F) were utilized in syngeneic immunocompetent mice. The prevalence of G-MDSCs in the TME of these tumors strongly correlated with the expression levels of ELR+ CXC chemokines in the corresponding cell lines (r=0.92) (Fig. 3G and Supplementary Fig. S2E).

We then evaluated the kinetics of peripheral G-MDSC accumulation in mice bearing KPL and KP tumors. A gradual enrichment of G-MDSCs was observed in the blood of mice from day 9 to day 14 after tumor inoculation, with a higher accumulation of G-MDSCs in mice bearing KPL tumors compared to the KP tumor-bearing mice (Fig. 3H). Similarly, splenic G-MDSCs were more abundant in tumor-bearing KPL mice compared to KP mice (Fig. 3I). A higher percentage of $CXCR2^{+}$G-MDSCs was observed in the blood and the spleen of KPL tumor-bearing mice compared to that of KP tumor-bearing mice (Supplementary Fig. S2F). A heightened level of circulating CXCL1 protein was also observed in the blood of mice with KPL tumors compared to those with KP tumors (Supplementary Fig. S2G). These data suggest that LKB1 deficiency in murine models of NSCLC leads to a heightened production of ELR+ CXC chemokines and is associated with local and systemic enrichment of G-MDSCs.

G-MDSC depletion enhances the proliferation and function of TILs, and potentiates the efficacy of anti-PD-1 therapy in LKB1-deficient NSCLC

MDSCs have emerged as potent suppressive immune mediators that facilitate tumorigenesis, metastasis, and resistance to therapy(32). We hypothesized that G-MDSCs mediate resistance to anti-PD-1 therapy in LKB1-deficient murine NSCLC. To test this hypothesis, the capacity of G-MDSC depletion via antibody to enhance the efficacy of anti-PD-1 therapy was evaluated in syngeneic murine models bearing 1940A KPL tumors (designated as KPL-P) that contain abundant G-MDSCs (Fig. 3G). No anti-tumor efficacy was observed with anti-Gr-1 and anti-PD-1 mono- or combination therapy (Supplementary Fig. S3A). The lack of efficacy in this study could be due to the paucity of tumor neoantigens, given that GEMMs of NSCLC possess low TMB(33,34). Therefore, 1940A KPL cells with increased TMB (designated as KPL-3M), induced by *in vitro* exposure to the carcinogen *N*-methyl-*N*-nitrosourea (MNU), were utilized(18). KPL-3M cells had analogous expression of *Cxcl1*, *Cxcl3*, *Cxcl5*, and *Cxcl7* chemokines compared to KPL-P cells, and an increase in *Cxcl2* expression (Supplementary Fig. S3B). Anti-PD-1 monotherapy in KPL-3M tumor-bearing mice elicited limited efficacy and anti-Gr-1 monotherapy did not affect tumor growth, however, combination therapy with anti-Gr-1 and anti-PD-1 resulted in a synergistic anti-tumor effect leading to a complete eradication of 88% of tumors and growth stabilization of remaining tumors (Fig. 4A).

To understand the mechanisms of the anti-tumor immunity in this model, tumors were immunophenotyped 10 days after treatment initiation when tumor weights were comparable (Supplementary Fig. S3C). Treatment with anti-Gr-1 antibody led to a robust depletion of tumor-infiltrating G-MDSCs (Fig. 4B). To account for the variability introduced by G-MDSC depletion, each immune cell subtype was normalized relative to the number of tumor

cells. Anti-Gr-1 treatment did not lead to changes in tumor-associated macrophages (TAMs), conventional DCs (cDCs), natural killer (NK) cells, FOXP3$^-$CD4 or CD8 T cells in the TME (Fig. 4B), but it did enhance the proliferation and function of FOXP3$^-$CD4 and CD8 tumor infiltrating lymphocytes (TILs), as determined by intracellular staining of Ki-67 and TNFα/IFNγ, respectively (Fig. 4C). Anti-Gr-1 monotherapy also enhanced NK proliferation and IFNγ secretion (Fig. 4D). Anti-PD-1 monotherapy also led to an increase in CD8 T cells secreting TNFα and IFNγ (Fig. 4C). Combination therapy with anti-Gr-1 and anti-PD-1 resulted in a significant decrease of G-MDSCs compared to the control, although not as robust as anti-Gr-1 monotherapy (Fig. 4B). A significant increase was observed in TAMs, cDCs, NKs, FOXP3$^-$CD4 and CD8 T cells following combination therapy (Fig. 4B). Importantly, combination therapy resulted in the most significant improvement in proliferation and cytokine secretions of both NK and T cells (Fig. 4C and 4D). This observation is consistent with the robust anti-tumor immunity observed in response to combination therapy. Upregulation of PD-L1 in tumor cells was also noted following all treatments, with the highest magnitude observed with combination therapy (Fig. 4E). These data suggest that G-MDSC depletion via anti-Gr-1 antibody enhances the proliferation and function of TILs and sensitizes LKB1-deficient tumors to anti-PD-1 therapy.

ATRA potentiates the efficacy of anti-PD-1 therapy in LKB1-deficient NSCLC

ATRA was assessed to determine if a pharmacological agent that interferes with MDSC function could be implemented to overcome resistance to anti-PD-1 in LKB1-deficient NSCLC. ATRA alters MDSC function via down regulation of deleterious reactive oxygen species (ROS)(35). Combination therapy with ATRA and anti-PD-1 resulted in robust anti-tumor efficacy with the eradication of over 70% of KPL-3M tumors (8/11) and the growth stabilization of remaining tumors (Fig. 5A). ATRA monotherapy led to modest efficacy similar to that of anti-PD-1 monotherapy.

Because ATRA can potentially inhibit tumor proliferation, studies were performed to determine whether the efficacy of ATRA monotherapy in this model is driven by the immune-modulatory effect of ATRA or its direct inhibition of tumor growth. Treatment of KPL-3M cells with ATRA *in vitro* did not inhibit tumor cell proliferation (Supplementary Fig. S4). Similarly, no differences in tumor growth were observed in KPL-3M tumor-bearing immunodeficient NSG mice treated with either vehicle or ATRA (Fig. 5B). These data suggest that the reduction of tumor growth by ATRA in immunocompetent mice is predominantly immune-mediated.

ATRA therapy suppresses the proliferation and function of G-MDSCs and leads to enhanced T cell infiltration, proliferation and activation in the TME of LKB1-deficient NSCLC

To assess the immune determinants of response to ATRA and combination therapy, the immune composition of the TME was evaluated 12 days following the initiation of treatment when tumor weights were generally comparable (Supplementary Fig. S5A). Evaluation of the myeloid compartment of the TME (Supplementary Fig. S5B) revealed that ATRA and anti-PD-1 mono- and combination therapies resulted in decreased G-MDSCs with the largest magnitude change observed in combination therapy (Fig 6A). ATRA monotherapy

did not lead to changes in the frequency of M-MDSC, TAM, cDC1, cDC2, or monocyte-derived inflammatory DC (inf DC) compared to vehicle control (Supplementary Fig. S5C). There was a significant increase in M-MDSCs and TAMs upon ATRA and anti-PD-1 combination therapy compared to vehicle control, but no difference in the DC populations (Supplementary Fig. S5C).

Within the lymphoid compartment of the TME, ATRA and anti-PD-1 mono- and combination therapy led to a significant increase in NK cells and TILs, including CD8, $FOXP3^{-}CD4$, and $CD4^{+}CD25^{+}FOXP3^{+}$ regulatory T (Treg) cells (Fig. 6B). The increase in TILs and NK cells was most pronounced in the combination group. The activation, proliferation and function of TILs were also assessed. ATRA monotherapy increased the number of $CD44^{+}PD\text{-}1^{+}TIM3^{-}FOXP3^{-}CD4$ and $CD44^{+}PD\text{-}1^{+}TIM3^{-}CD8$ T cells, which represent activated antigen-experienced TILs that are not terminally exhausted(36) (Fig. 6C). Combination therapy of ATRA and anti-PD-1 resulted in a greater increase in these populations compared to ATRA monotherapy. ATRA alone and in combination with anti-PD-1 enhanced the proliferation of CD4 and CD8 TILs, with the greatest increase noted in the combination group (Fig. 6D). ATRA and anti-PD-1 combination therapy also led to a significantly higher percentage of $PD\text{-}1^{+}FOXP3^{-}CD4$ and $PD\text{-}1^{+}CD8$ T cells secreting TNFα and IFNγ (Fig. 6E). Increased proliferation and IFNγ secretion were also noted in tumor-infiltrating NK cells following combination therapy (Fig. 6F). Similarly, the highest magnitude of PD-L1 upregulation by tumor and myeloid cells was observed in the ATRA and anti-PD-1 combination group (Supplemental Fig. S5D and S5E). These data suggest that ATRA therapy increases TILs and enhances their activation and proliferation. The addition of anti-PD-1 to ATRA therapy results in further enhancement of the proliferation and augmentation of the effector function of these TILs.

To assess whether ATRA modulation of G-MDSCs mediated the observed enhancement of T cell proliferation in the TME, tumor-infiltrating G-MDSCs from KPL-3M tumor-bearing mice treated with ATRA or vehicle were flow-sorted. Co-culturing of G-MDSCs with T cells revealed that G-MDSCs from ATRA-treated tumor-bearing mice had reduced T cell suppressive capacity compared to G-MDSCs from untreated tumor-bearing control mice (Fig. 6G). Similarly, *in vitro* ATRA treatment of G-MDSCs from control mice diminished the suppression of T cell proliferation compared to untreated G-MDSCs (Supplemental Fig. S5F). ATRA also exhibited a minor inhibition on GMDSC proliferation *in vitro* (Supplementary Fig. S5G). These data suggest that ATRA-induced potentiation of anti-PD-1 efficacy is partially mediated through direct ATRA suppression of G-MDSC proliferation and function.

Combination therapy with ATRA and anti-PD-1 induces systemic tumor-specific immune memory

A significant reduction in G-MDSCs and M-MDSCs was observed in the spleen of KPL-3M tumor-bearing mice following ATRA monotherapy and combination therapy, but this was not evident with anti-PD-1 monotherapy (Fig. 7A). No difference was noted in the frequency of macrophages with treatments (Supplemental Fig. S6A). Evaluation of the T cell subgroups in the spleen revealed no differences in the overall abundance of $FOXP3^{-}$

CD4, CD8 or Tregs following any treatment (Supplementary Fig. S6B). An increase in $CD44^+CD62L^-$ effector memory (EM) T cells with a higher percentage of PD-1^+ cells was observed within the $FOXP3^-$CD4 T cell population, following anti-PD-1 mono- or combination therapy (Fig. 7B). Neither the proliferation nor the cytokine secretion (TNFα and IFNγ) of PD-1^+EM CD4 cells were altered by therapy (Fig. 7B and Supplementary Fig. S6C). There was no difference in the overall frequency of CD8 EM T cell populations among treatment groups, but a higher percentage of PD-1^+ cells was observed within the CD8 EM T cell population following anti-PD-1 mono- or combination therapy (Fig. 7C). No difference in the proliferation of PD-1^+ CD8 EM cells was observed following treatments, but ATRA mono- and combination therapy resulted in an increase in cytokine-secreting cells (Fig. 7C and Supplemental Fig. S6D). A higher percentage of $CD44^+CD62L^+$ central memory (CM) CD8 T cells was found in response to ATRA and anti-PD-1 combination therapy. CM CD8 cells demonstrated enhanced proliferation following ATRA and anti-PD-1 mono- or combination therapy (Fig. 7D). A significantly higher level of IFNγ secretion in splenic NK cells was also noted following ATRA mono- or combination therapy (Supplementary Fig S6E). These data provide compelling evidence that combination therapy with ATRA and anti-PD-1 results in enhanced systemic T cell responses in KPL-3M tumor-bearing mice.

Next, we assessed whether the anti-tumor efficacy associated with combination therapy of ATRA and anti-PD-1 resulted in the establishment of systemic tumor-specific T cell immunity. Mice with complete tumor eradication following therapy with ATRA and anti-PD-1 combination were re-challenged with KPL-3M cells three months after the complete anti-tumor response. Naïve mice were included as controls. While naïve mice succumbed to tumor progression, the re-challenged mice eradicated 100% of tumors following an initial tumor growth (Fig. 7E). In contrast, a secondary challenge with a distinct cancer cell line from the same FVB background (MyC-CaP) resulted in tumor growth in all the cured and naïve control mice (Fig. 7F). These data indicate that ATRA therapy in combination with anti-PD-1 elicits durable systemic anti-tumor immunity.

Discussion

Loss of *LKB1* is a primary driver of resistance to anti-PD-1 therapy in *KRAS*-mutant NSCLC(13). Studies indicate that inactivation of LKB1 in NSCLC is associated with a distinct TME characterized by diminished T cell infiltration, low or absent PD-L1 expression, and abundance of neutrophils(12–14). Our work extends the previous studies in several key areas. We report that: (1) LKB1 is a negative regulator of ELR+ CXC chemokine transcription in HBECs, murine and human NSCLC cells; (2) Heightened levels of ELR+ CXC chemokines in murine LKB1-deficient NSCLC models correlate with increased systemic and local G-MDSC enrichment; (3) Depletion of G-MDSCs via anti-Gr-1 antibody or their functional inhibition via ATRA activates TILs and sensitizes LKB1-deficent tumors to PD-1 blockade; (4) Anti-PD-1 combined with ATRA therapy induces durable anti-tumor T cell responses and systemic anti-tumor immunity. These findings enhance our understanding of the critical mediators of immunosuppression in LKB1-deficient NSCLC and provide preclinical evidence for combining PD-1 blockade with therapies that interfere with MDSCs.

Although prior murine and human studies reveal an enrichment of neutrophils in LKB1-deficient NSCLC(12,14), the molecular mediators of this phenotype are not well understood. Koyama et al. identified that loss of LKB1 in murine models of NSCLC results in an increased secretion of cytokines involved in neutrophil production and accumulation, including G-CSF, IL-6 and CXCL7(12). Our findings further establish LKB1 as a negative regulator of the ELR+ CXC chemokine family in HBECs as well as murine and human lung cancer cell lines. We found a robust positive correlation between the increased tumor expression of ELR+ CXC chemokines and the frequency of G-MDSCs in the TME and the periphery of tumor-bearing mice, implicating ELR+ CXC chemokines as potential mediators of G-MDSC/neutrophil accumulation in LKB1-deficient NSCLC. Previous studies have revealed Hippo and Wnt signaling as two oncogenic pathways downstream of LKB1 that regulate ELR+ CXC chemokines(37–41). Future mechanistic studies are necessary to delineate the specific molecular mechanisms of LKB1-mediated regulation of ELR+ CXC chemokines in NSCLC.

Our current studies support the hypothesis that G-MDSC accumulation mediates resistance to immunotherapy in LKB1-defecient murine NSCLC. This is supported by the finding that G-MDSC depletion via anti-Gr-1 antibody resulted in improved proliferation and cytotoxic function of NK and T cells in the TME and sensitized LKB1-deficient tumors to anti-PD-1 therapy. This hypothesis is further corroborated by clinical studies in NSCLC patients that implicate G-MDSC/neutrophil and ELR+ CXC chemokines as mediators of resistance to ICIs. Kim et al. demonstrated that a high frequency of circulating LOX-1^{+} G-MDSCs and low frequency of Treg cells in patients with NSCLC are associated with a decreased progression free survival following treatment with Nivolumab(42). Kargl *et al* reported that neutrophils are negatively correlated with CD4 and CD8 T cell content in NSCLC TME(43), and that a high neutrophil to CD8 T cell ratio is associated with worse outcomes in NSCLC patients treated with ICIs(44). A recent report by Schalper et al. demonstrated that NSCLC patients with elevated serum levels of CXCL8 have greater accumulation of intratumoral neutrophils and reduced clinical benefits in response to ICIs(45). Consistent with these findings, there are several early phase clinical trials in NSCLC evaluating the combination of ICIs with therapies that target G-MDSC/neutrophil trafficking into tumors(46).

We speculated that pharmacological treatment with ATRA would allow for a translatable approach to ameliorate MDSC-mediated immunosuppression and augment host anti-tumor immune responses. ATRA is a widely utilized drug that induces the differentiation of immature myelocytic cells and is a standard component of induction therapy for patients with acute promyelocytic leukemia(47). Our studies in the KPL-3M murine model revealed that ATRA synergized with anti-PD-1 and resulted in systemic tumor-specific immunity. Mechanistically, ATRA did not appear to have direct anti-tumor cytotoxicity, based on the lack of *in vivo* efficacy in NSG mice and the absence of inhibition on tumor proliferation *in vitro*. In the immunocompetent models, treatment with ATRA resulted in profound remodeling of the local and systemic immune landscape, including a reduction in splenic and tumor G-MDSCs, and an increase in tumor-infiltrating NK cells and antigen-experienced TILs with an enhanced proliferation capacity. Our studies provide compelling evidence that the effic00acy of ATRA treatment in LKB1-deficient NSCLC is partially mediated through ATRA-mediated suppression of G-MDSC proliferation and

function. These results add to the previous reports demonstrating that ATRA can promote differentiation of MDSC into macrophages and DCs and decrease the suppressive effects of MDSCs (35,48,49).

In summary, we report that loss of LKB1 in NSCLC induces heightened production of ELR+ CXC chemokines. The abundance of ELR+ CXC chemokines in LKB1-deficient NSCLC murine models correlates with an enrichment of G-MDSCs, which drives resistance to anti-PD-1 therapy. The removal of G-MDSC-mediated immunosuppression via depletion with anti-Gr-1 antibody, or functional inhibition with ATRA, restores anti-tumor T cell responses and sensitizes resistant LKB1-deficient NSCLC to anti-PD-1 therapy. These results provide preclinical evidence in support of the clinical investigation of ATRA therapy to augment the efficacy of anti-PD-1 immunotherapy in patients with LKB-1 deficient NSCLC.

Supplementary Material

Refer to Web version on PubMed Central for supplementary material.

Acknowledgements:

The authors thank John Minna for providing HBEC lines and both Lauren Winter and Tamara Silva for administrative support.

Financial Support: This research was supported in part by funding from the National Cancer Institute (1U01-CA196408), National Heart Lung and Blood Institute (T32-HL072752), Medical Research Funds from the Department of Veteran Affairs, and NIH/NCATS UL1TR001881. The UCLA Jonsson Comprehensive Cancer Center (JCCC) and Center for AIDS Research Flow Cytometry Core is supported by the National Institutes of Health (NIH; #CA-16042 and #AI-28697).

References:

1. Reck M, Rodriguez-Abreu D, Robinson AG, Hui R, Csoszi T, Fulop A, et al. Pembrolizumab versus Chemotherapy for PD-L1-Positive Non-Small-Cell Lung Cancer. N Engl J Med 2016;375:1823–33 [PubMed: 27718847]
2. Gandhi L, Rodríguez-Abreu D, Gadgeel S, Esteban E, Felip E, De Angelis F, et al. Pembrolizumab plus Chemotherapy in Metastatic Non–Small-Cell Lung Cancer. N Engl J Med 2018;378:2078–92 [PubMed: 29658856]
3. Paz-Ares L, Luft A, Vicente D, Tafreshi A, Gumus M, Mazieres J, et al. Pembrolizumab plus Chemotherapy for Squamous Non-Small-Cell Lung Cancer. N Engl J Med 2018;379:2040–51 [PubMed: 30280635]
4. Reck M, Rodriguez-Abreu D, Robinson AG, Hui R, Csoszi T, Fulop A, et al. Updated Analysis of KEYNOTE-024: Pembrolizumab Versus Platinum-Based Chemotherapy for Advanced Non-Small-Cell Lung Cancer With PD-L1 Tumor Proportion Score of 50% or Greater. J Clin Oncol 2019;37:537–46 [PubMed: 30620668]
5. Garon EB, Hellmann MD, Rizvi NA, Carcereny E, Leighl NB, Ahn MJ, et al. Five-Year Overall Survival for Patients With Advanced NonSmall-Cell Lung Cancer Treated With Pembrolizumab: Results From the Phase I KEYNOTE-001 Study. J Clin Oncol 2019;37:2518–27 [PubMed: 31154919]
6. Tumeh PC, Harview CL, Yearley JH, Shintaku IP, Taylor EJ, Robert L, et al. PD-1 blockade induces responses by inhibiting adaptive immune resistance. Nature 2014;515:568–71 [PubMed: 25428505]
7. Garon EB, Rizvi NA, Hui R, Leighl N, Balmanoukian AS, Eder JP, et al. Pembrolizumab for the treatment of non-small-cell lung cancer. N Engl J Med 2015;372:2018–28 [PubMed: 25891174]

8. Rizvi NA, Hellmann MD, Snyder A, Kvistborg P, Makarov V, Havel JJ, et al. Cancer immunology. Mutational landscape determines sensitivity to PD-1 blockade in non-small cell lung cancer. Science 2015;348:124–8 [PubMed: 25765070]
9. McGranahan N, Furness AJ, Rosenthal R, Ramskov S, Lyngaa R, Saini SK, et al. Clonal neoantigens elicit T cell immunoreactivity and sensitivity to immune checkpoint blockade. Science 2016;351:1463–9 [PubMed: 26940869]
10. Skoulidis F, Heymach JV. Co-occurring genomic alterations in non-small-cell lung cancer biology and therapy. Nature reviews Cancer 2019;19:495–509 [PubMed: 31406302]
11. Shackelford DB, Shaw RJ. The LKB1-AMPK pathway: metabolism and growth control in tumour suppression. Nature reviews Cancer 2009;9:563–75
12. Koyama S, Akbay EA, Li YY, Aref AR, Skoulidis F, Herter-Sprie GS, et al. STK11/LKB1 Deficiency Promotes Neutrophil Recruitment and Proinflammatory Cytokine Production to Suppress T-cell Activity in the Lung Tumor Microenvironment. Cancer Res 2016;76:999–1008 [PubMed: 26833127]
13. Skoulidis F, Goldberg ME, Greenawalt DM, Hellmann MD, Awad MM, Gainor JF, et al. STK11/LKB1 Mutations and PD-1 Inhibitor Resistance in KRAS-Mutant Lung Adenocarcinoma. Cancer Discov 2018;8:822–35 [PubMed: 29773717]
14. Gillette MA, Satpathy S, Cao S, Dhanasekaran SM, Vasaikar SV, Krug K, et al. Proteogenomic Characterization Reveals Therapeutic Vulnerabilities in Lung Adenocarcinoma. Cell 2020;182:200–25 e35 [PubMed: 32649874]
15. Ramirez RD, Sheridan S, Girard L, Sato M, Kim Y, Pollack J, et al. Immortalization of human bronchial epithelial cells in the absence of viral oncoproteins. Cancer Res 2004;64:9027–34 [PubMed: 15604268]
16. Pagano PC, Tran LM, Bendris N, O'Byrne S, Tse HT, Sharma S, et al. Identification of a Human Airway Epithelial Cell Subpopulation with Altered Biophysical, Molecular, and Metastatic Properties. Cancer Prev Res 2017;10:514–24
17. Sato M, Vaughan MB, Girard L, Peyton M, Lee W, Shames DS, et al. Multiple oncogenic changes (K-RAS(V12), p53 knockdown, mutant EGFRs, p16 bypass, telomerase) are not sufficient to confer a full malignant phenotype on human bronchial epithelial cells. Cancer Res 2006;66:2116–28 [PubMed: 16489012]
18. Salehi-Rad R, Li R, Tran LM, Lim RJ, Abascal J, Momcilovic M, et al. Novel Kras-mutant murine models of non-small cell lung cancer possessing co-occurring oncogenic mutations and increased tumor mutational burden. Cancer Immunol Immunother 2021. doi: 10.1007/s00262-020-02837-9
19. Li R, Ong SL, Tran LM, Jing Z, Liu B, Park SJ, et al. Chronic IL-1beta-induced inflammation regulates epithelial-to-mesenchymal transition memory phenotypes via epigenetic modifications in non-small cell lung cancer. Sci Rep 2020;10:377 [PubMed: 31941995]
20. Shackelford DB, Abt E, Gerken L, Vasquez DS, Seki A, Leblanc M, et al. LKB1 inactivation dictates therapeutic response of non-small cell lung cancer to the metabolism drug phenformin. Cancer Cell 2013;23:143–58 [PubMed: 23352126]
21. Momcilovic M, Bailey ST, Lee JT, Zamilpa C, Jones A, Abdelhady G, et al. Utilizing 18F-FDG PET/CT Imaging and Quantitative Histology to Measure Dynamic Changes in the Glucose Metabolism in Mouse Models of Lung Cancer. J Vis Exp 2018
22. Tekpli X, Landvik NE, Anmarkud KH, Skaug V, Haugen A, Zienolddiny S. DNA methylation at promoter regions of interleukin 1B, interleukin 6, and interleukin 8 in non-small cell lung cancer. Cancer Immunol Immunother 2013;62:337–45 [PubMed: 22923190]
23. Cheung HH, Lee TL, Davis AJ, Taft DH, Rennert OM, Chan WY. Genome-wide DNA methylation profiling reveals novel epigenetically regulated genes and non-coding RNAs in human testicular cancer. Br J Cancer 2010;102:419–27 [PubMed: 20051947]
24. Barretina J, Caponigro G, Stransky N, Venkatesan K, Margolin AA, Kim S, et al. The Cancer Cell Line Encyclopedia enables predictive modelling of anticancer drug sensitivity. Nature 2012;483:603–7 [PubMed: 22460905]
25. Ji H, Houghton AM, Mariani TJ, Perera S, Kim CB, Padera R, et al. K-ras activation generates an inflammatory response in lung tumors. Oncogene 2006;25:2105–12 [PubMed: 16288213]

26. Sunaga N, Kaira K, Tomizawa Y, Shimizu K, Imai H, Takahashi G, et al. Clinicopathological and prognostic significance of interleukin-8 expression and its relationship to KRAS mutation in lung adenocarcinoma. Br J Cancer 2014;110:2047–53 [PubMed: 24577055]
27. Chao T, Furth EE, Vonderheide RH. CXCR2-Dependent Accumulation of Tumor-Associated Neutrophils Regulates T-cell Immunity in Pancreatic Ductal Adenocarcinoma. Cancer Immunol Res 2016;4:968–82 [PubMed: 27737879]
28. Ignacio RMC, Gibbs CR, Lee ES, Son DS. The TGFalpha-EGFR-Akt signaling axis plays a role in enhancing proinflammatory chemokines in triple-negative breast cancer cells. Oncotarget 2018;9:29286–303 [PubMed: 30034618]
29. Whipple CA, Brinckerhoff CE. BRAF(V600E) melanoma cells secrete factors that activate stromal fibroblasts and enhance tumourigenicity. Br J Cancer 2014;111:1625–33 [PubMed: 25117819]
30. Cheng Y, Ma XL, Wei YQ, Wei XW. Potential roles and targeted therapy of the CXCLs/CXCR2 axis in cancer and inflammatory diseases. Biochim Biophys Acta Rev Cancer 2019;1871:289–312 [PubMed: 30703432]
31. Eash KJ, Greenbaum AM, Gopalan PK, Link DC. CXCR2 and CXCR4 antagonistically regulate neutrophil trafficking from murine bone marrow. J Clin Invest 2010;120:2423–31 [PubMed: 20516641]
32. Veglia F, Perego M, Gabrilovich D. Myeloid-derived suppressor cells coming of age. Nat Immunol 2018;19:108–19 [PubMed: 29348500]
33. Westcott PM, Halliwill KD, To MD, Rashid M, Rust AG, Keane TM, et al. The mutational landscapes of genetic and chemical models of Kras-driven lung cancer. Nature 2015;517:489–92 [PubMed: 25363767]
34. McFadden DG, Politi K, Bhutkar A, Chen FK, Song X, Pirun M, et al. Mutational landscape of EGFR-, MYC-, and Kras-driven genetically engineered mouse models of lung adenocarcinoma. Proc Natl Acad Sci 2016;113:E6409–E17 [PubMed: 27702896]
35. Nefedova Y, Fishman M, Sherman S, Wang X, Beg AA, Gabrilovich DI. Mechanism of all-trans retinoic acid effect on tumor-associated myeloid-derived suppressor cells. Cancer Res 2007;67:11021–8 [PubMed: 18006848]
36. Wherry EJ, Kurachi M. Molecular and cellular insights into T cell exhaustion. Nat Rev Immunol 2015;15:486–99 [PubMed: 26205583]
37. Ossipova O, Bardeesy N, DePinho RA, Green JB. LKB1 (XEEK1) regulates Wnt signalling in vertebrate development. Nat Cell Biol 2003;5:889–94 [PubMed: 12973359]
38. Jacob LS, Wu X, Dodge ME, Fan CW, Kulak O, Chen B, et al. Genome-wide RNAi screen reveals disease-associated genes that are common to Hedgehog and Wnt signaling. Sci Signal 2011;4:ra4
39. Levy L, Neuveut C, Renard CA, Charneau P, Branchereau S, Gauthier F, et al. Transcriptional activation of interleukin-8 by beta-catenin-Tcf4. J Biol Chem 2002;277:42386–93 [PubMed: 12200448]
40. Rauner M, Stein N, Winzer M, Goettsch C, Zwerina J, Schett G, et al. WNT5A is induced by inflammatory mediators in bone marrow stromal cells and regulates cytokine and chemokine production. J Bone Miner Res 2012;27:575–85 [PubMed: 22162112]
41. Wang G, Lu X, Dey P, Deng P, Wu CC, Jiang S, et al. Targeting YAP-Dependent MDSC Infiltration Impairs Tumor Progression. Cancer Discov 2016;6:80–95 [PubMed: 26701088]
42. Kim HR, Park SM, Seo SU, Jung I, Yoon HI, Gabrilovich DI, et al. The Ratio of Peripheral Regulatory T Cells to Lox-1(+) Polymorphonuclear Myeloid-derived Suppressor Cells Predicts the Early Response to Anti-PD-1 Therapy in Patients with Non-Small Cell Lung Cancer. Am J Respir Crit Care Med 2019;199:243–6 [PubMed: 30339766]
43. Kargl J, Busch SE, Yang GH, Kim KH, Hanke ML, Metz HE, et al. Neutrophils dominate the immune cell composition in non-small cell lung cancer. Nat Commun 2017;8:14381 [PubMed: 28146145]
44. Kargl J, Zhu X, Zhang H, Yang GHY, Friesen TJ, Shipley M, et al. Neutrophil content predicts lymphocyte depletion and anti-PD1 treatment failure in NSCLC. JCI Insight 2019;4
45. Schalper KA, Carleton M, Zhou M, Chen T, Feng Y, Huang SP, et al. Elevated serum interleukin-8 is associated with enhanced intratumor neutrophils and reduced clinical benefit of immune-checkpoint inhibitors. Nat Med 2020;26:688–92 [PubMed: 32405062]

46. Hou A, Hou K, Huang Q, Lei Y, Chen W. Targeting Myeloid-Derived Suppressor Cell, a Promising Strategy to Overcome Resistance to Immune Checkpoint Inhibitors. Front Immunol 2020;11:783 [PubMed: 32508809]

47. Sanz MA, Fenaux P, Tallman MS, Estey EH, Lowenberg B, Naoe T, et al. Management of acute promyelocytic leukemia: updated recommendations from an expert panel of the European LeukemiaNet. Blood 2019;133:1630–43 [PubMed: 30803991]

48. Kusmartsev S, Cheng F, Yu B, Nefedova Y, Sotomayor E, Lush R, et al. All-trans-retinoic acid eliminates immature myeloid cells from tumor-bearing mice and improves the effect of vaccination. Cancer Res 2003;63:4441–9 [PubMed: 12907617]

49. Long AH, Highfill SL, Cui Y, Smith JP, Walker AJ, Ramakrishna S, et al. Reduction of MDSCs with All-trans Retinoic Acid Improves CAR Therapy Efficacy for Sarcomas. Cancer Immunol Res 2016;4:869–80 [PubMed: 27549124]

Significance:

Findings show that accumulation of myeloid-derived suppressor cells in LKB1-deficient non-small cell lung cancer can be overcome via treatment with all-trans-retinoic acid, sensitizing tumors to immunotherapy.

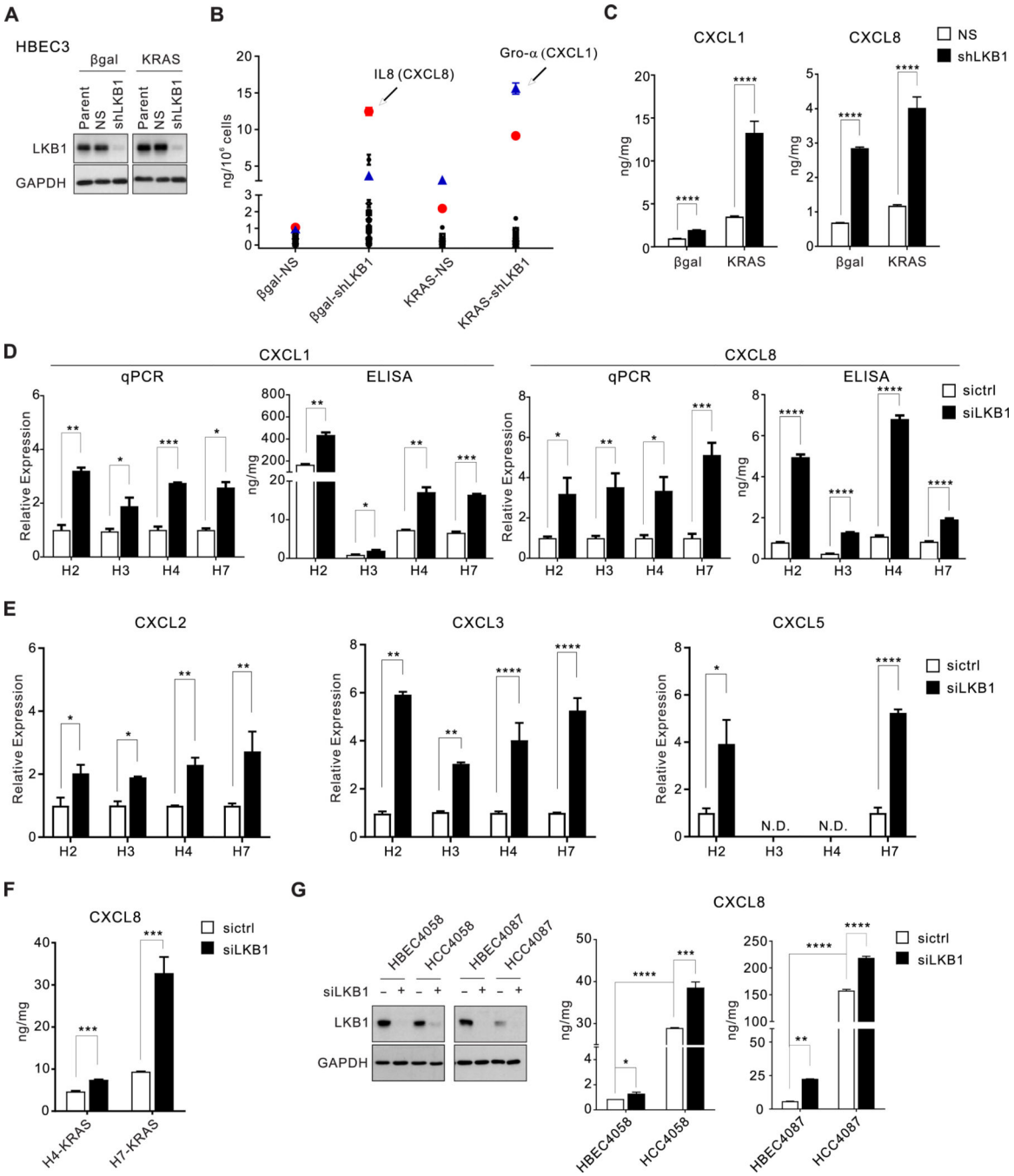

Figure 1. LKB1-loss induces the expression of ELR+ CXC chemokines in HBECs.

A) Immunoblotting of βgal or KRAS HBEC3 cell lines transduced with NS or shLKB1 lenti-virus. **B)** Bio-Plex screening of forty-five soluble factors from indicated isogenic HBEC3 cell lines. Each dot represents a soluble factor. **C**) CXCL1 and CXCL8 secretion by HBEC3 βgal and KRAS cells with or without LKB1 knockdown was determined by ELISA. **D**) Gene expression and protein secretion of CXCL1 and CXCL8 in H2, H3, H4, and H7 cells transfected with sictrl or siLKB1 were determined by q-PCR and ELISA, respectively. **E**) Relative gene expression of *CXCL2*, *CXCL3*, and *CXCL5* in the same cells as in **D** was

determined by q-PCR. *CXCL5* was not detectable (N.D.) in H3 and H4 cells. **F**) CXCL8 secretion in H4 and H7 KRAS cells following transient LKB1 knockdown was evaluated by ELISA. **G**) Immunoblotting of LKB1 in two sets of HBEC-HCC pair (left). CXCL8 secretion was evaluated by ELISA (right). *, $P<0.05$; **, $P< 0.01$; ***, $P<0.001$; ****, $P< 0.0001$.

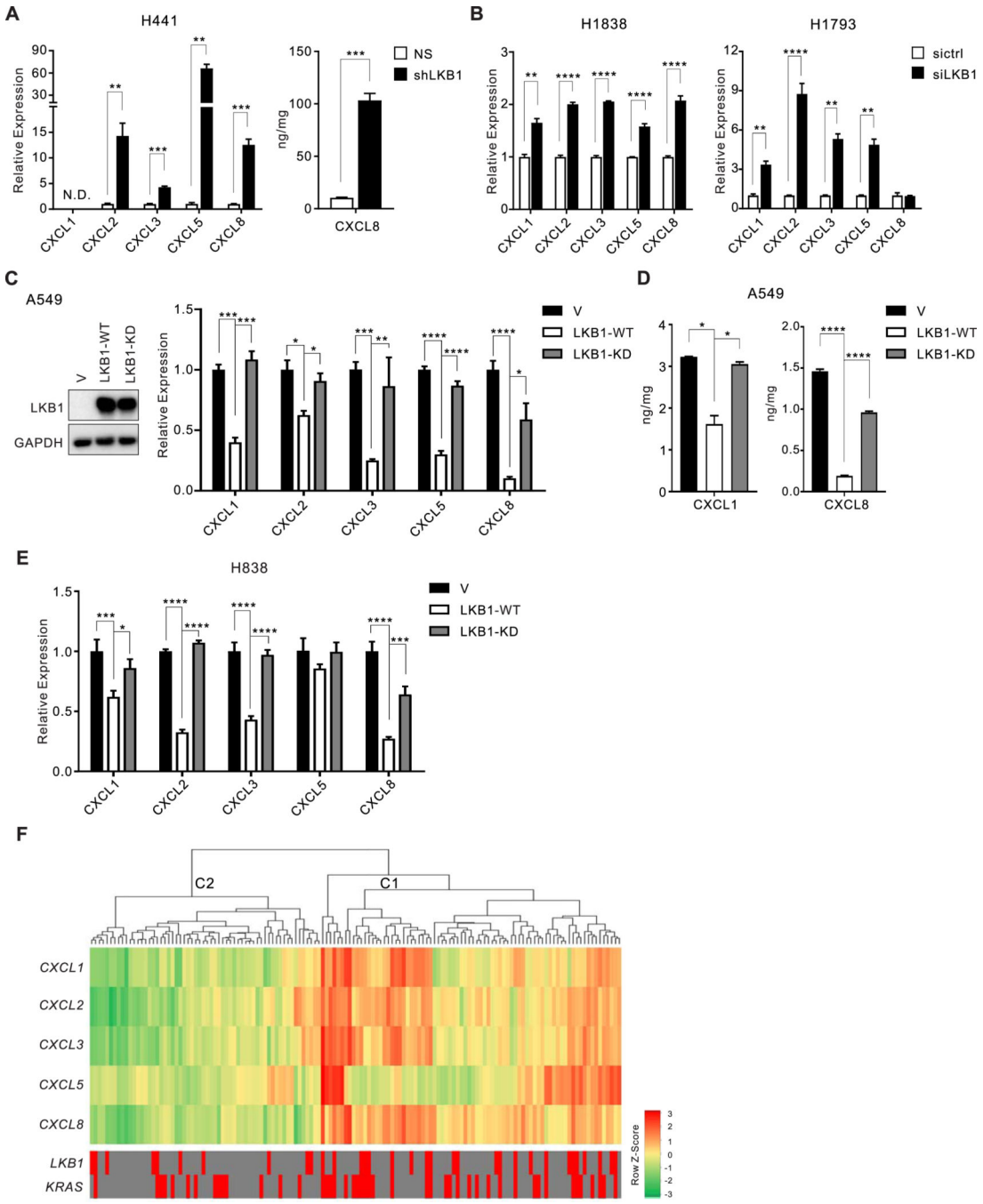

Figure 2. LKB1 regulates ELR+ CXC chemokines in human NSCLC cell lines.

A) Gene expression of the indicated ELR+ CXC chemokines was assessed by q-PCR in H441 cancer cells transduced with NS or shLKB1 lenti-virus (left). CXCL8 secretion was validated by ELISA (right). N.D., non-detectable. **B**) Gene expression of the indicated ELR+ CXC chemokines in H1838 and H1793 cancer cells with transient LKB1 knockdown. **C**) Expression of LKB1 by immunoblotting after reintroduction of WT-LKB1 or KD-LKB1 in A549 cells harboring intrinsic LKB1-deletion (left). Expression of the indicated ELR+ CXC chemokines in these isogenic cell lines by q-PCR (right). **D**) CXCL1 and CXCL8 secretion

in A549 isogenic cell lines were validated by ELISA. **E**) Expression of the indicated ELR+ CXC chemokines in isogenic H838 cell lines by q-PCR. **F**) Non-supervised clustering analysis of the indicated ELR+ CXC chemokine expression in 138 human NSCLC cell lines from the CCLE database. Cluster 1 (C1) represents cell lines with high chemokine expression while cluster 2 (C2) with low chemokine expression. *KRAS* and *LKB1* mutations were indicated by red shades below the heatmap. V, vector control. *, $P<0.05$; **, $P< 0.01$; ***, $P<0.001$; ****, $P< 0.0001$.

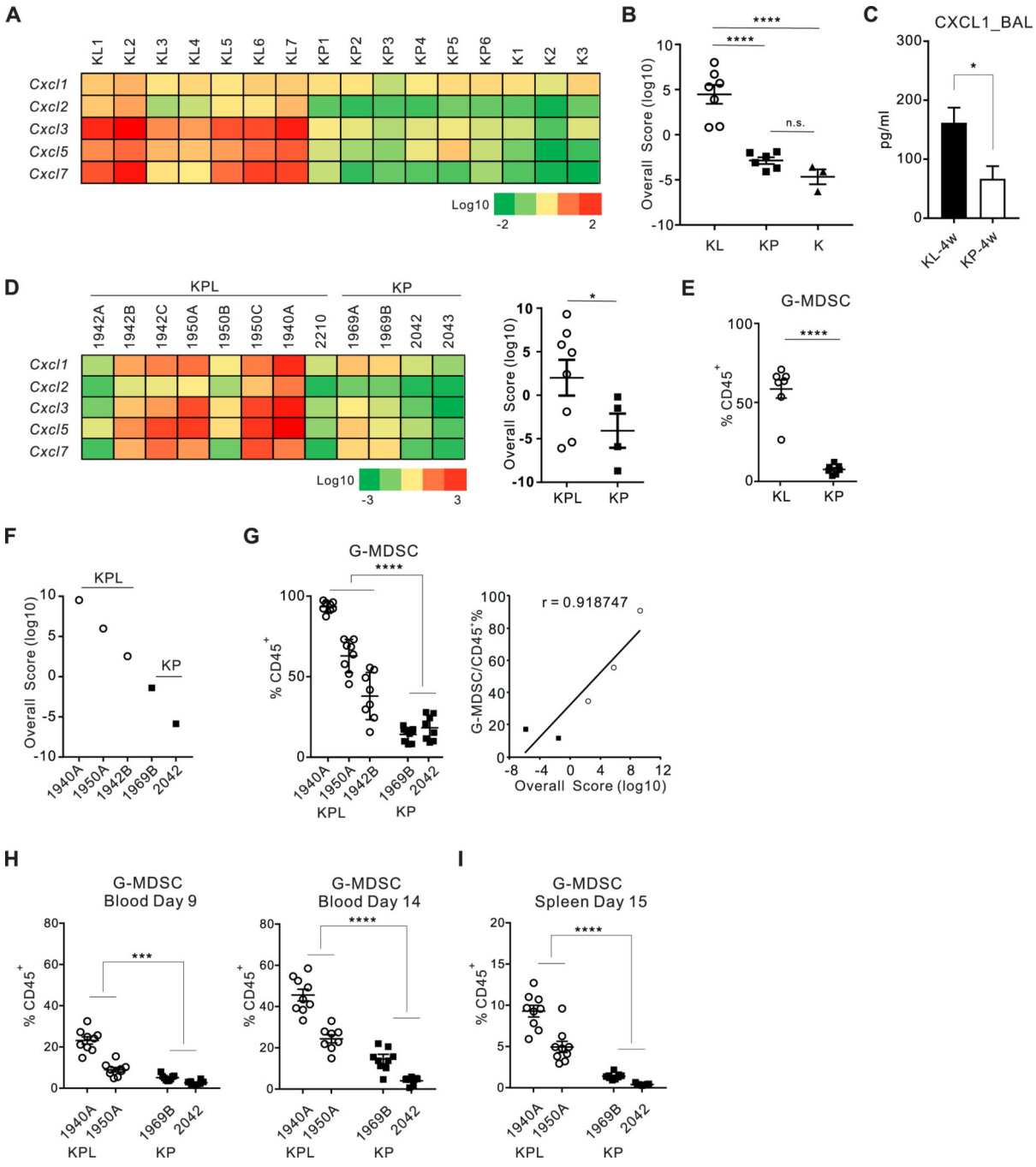

Figure 3. Heightened levels of ELR+ CXC chemokines in preclinical LKB1-deficient NSCLC tumors are associated with a G-MDSC-enriched microenvironment.

A) Relative gene expression of the indicated chemokines in multiple lung tumors from K, KP, and KL genetically-engineered mice was determined by q-PCR. Data are presented as a heatmap. **B**) The overall scores of the indicated chemokine expression in KL, KP, and K tumors are presented. **C**) CXCL1 concentration in bronchoalveolar lavage (BAL) fluid from KP and KL mice 4 weeks (4w) post tumor induction was evaluated by ELISA. Four mice per group were pooled and subjected to analysis. **D**) Heatmap of relative gene

expression of the indicated chemokines in the syngeneic murine NSCLC cell lines (left). The overall scores of ELR+ CXC chemokines from KPL and KP murine NSCLC cell lines (right). **E**) The abundance of G-MDSCs in lung tumors of KP and KL mice was determined by flow cytometry. G-MDSC is defined as $MHCII^{lo}CD11b^{+}Ly6C^{lo}Ly6G^{+}$. **F**) The overall ELR+ CXC chemokine scores of three KPL and two KP murine NSCLC cell lines. **G**) The abundance of G-MDSC within subcutaneous tumors derived from the same cells as in **F** (left), [1940A (1×10^5), 1950A (3×10^5), 1942B (1×10^6), 1969B (1×10^6), 2042 (1.5×10^6) cells in FBV mice]. The correlation between the overall score and G-MDSC percentage in KPL and KP tumors (p=0.027) (right). **H**) The abundance of G-MDSC in the blood of mice bearing subcutaneous KPL and KP tumors on day 9 and day 14. **I**) The abundance of G-MDSC in the spleen of mice bearing subcutaneous KPL and KP tumors on day 15 as in **G**. * $P<0.05$; **, $P< 0.01$; ***, $P<0.001$; ****, $P< 0.0001$. n.s., not significant.

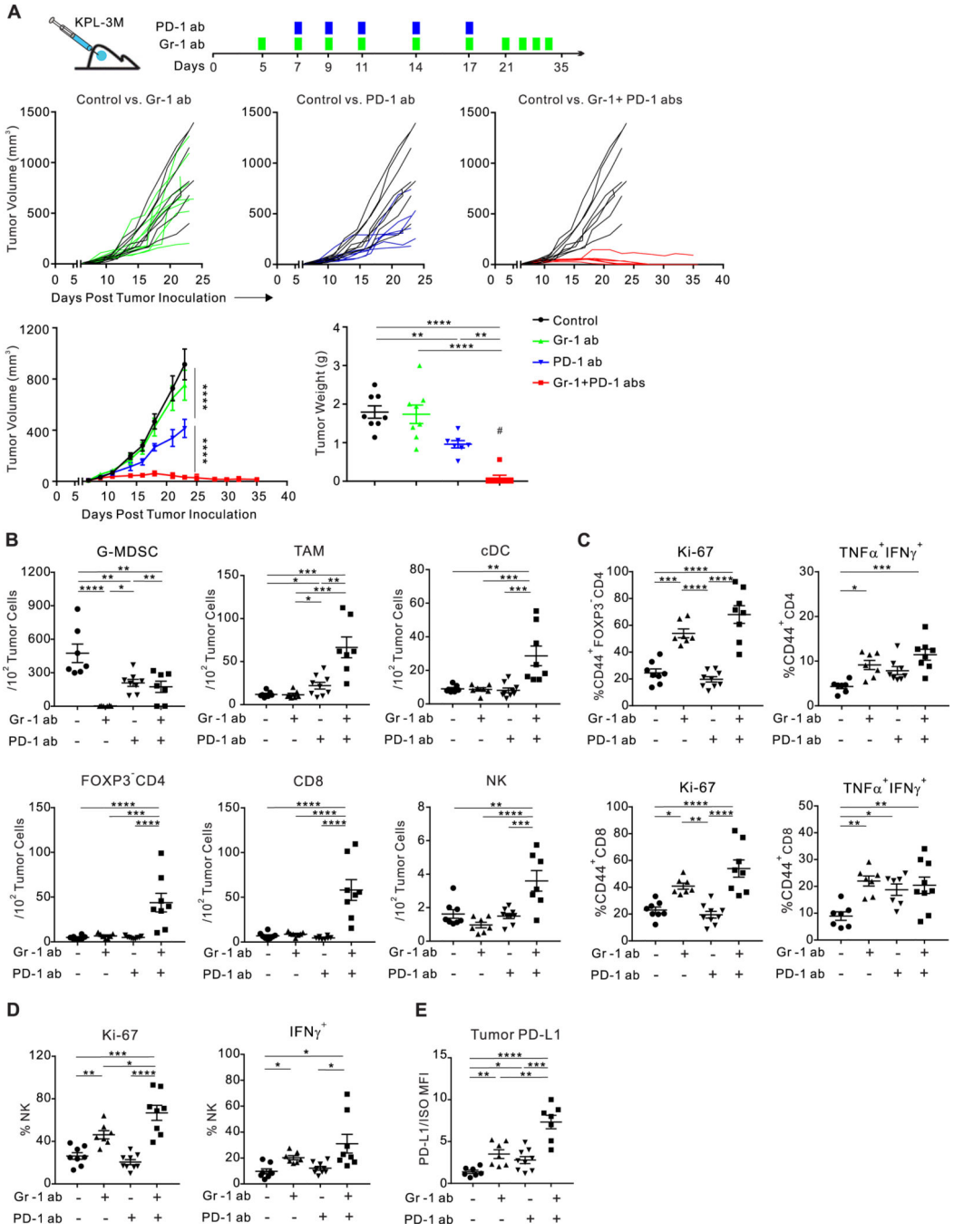

Figure 4. G-MDSC depletion enhances the proliferation and function of TILs, and potentiates the efficacy of anti-PD-1 therapy in LKB1-deficient NSCLC.

A) After subcutaneous inoculation of FVB mice with 1.5×10^5 KPL-3M cells, anti-Gr-1 (green box) treatment was started on day 5, and anti-PD-1 (blue box) therapy on day 7. Further doses were given as illustrated. Results are representative of at least three biological replicates of 6–10 mice per group. **B-E**) Similar experiments as in **A** were performed. Tumors and spleens were harvested on day 15 and analyzed by flow cytometry. **B**) The abundance of G-MDSC, tumor-associated macrophage (TAM), conventional dendritic cell

(cDC), FOXP^{-}CD4 and CD8 T cells, and NK cells is presented as per one hundred tumor cells in the TME determined with a gating strategy similar as in Fig. S5A. **C**) Proliferation (Ki67 staining) and cytokine secretion (TNFα and IFNγ staining) of tumor-infiltrating FOXP^{-}CD4 and CD8 T cells. **D**) Proliferation (Ki67 staining) and cytokine secretion (IFNγ staining) of tumor-infiltrating NK cells. **E**) Tumor PD-L1 expression presented as mean fluorescence intensity (MFI) normalized to isotype control (ISO). Treatment is indicated at the bottom of each graph. * P<0.05; **, P< 0.01; ****, P< 0.0001.

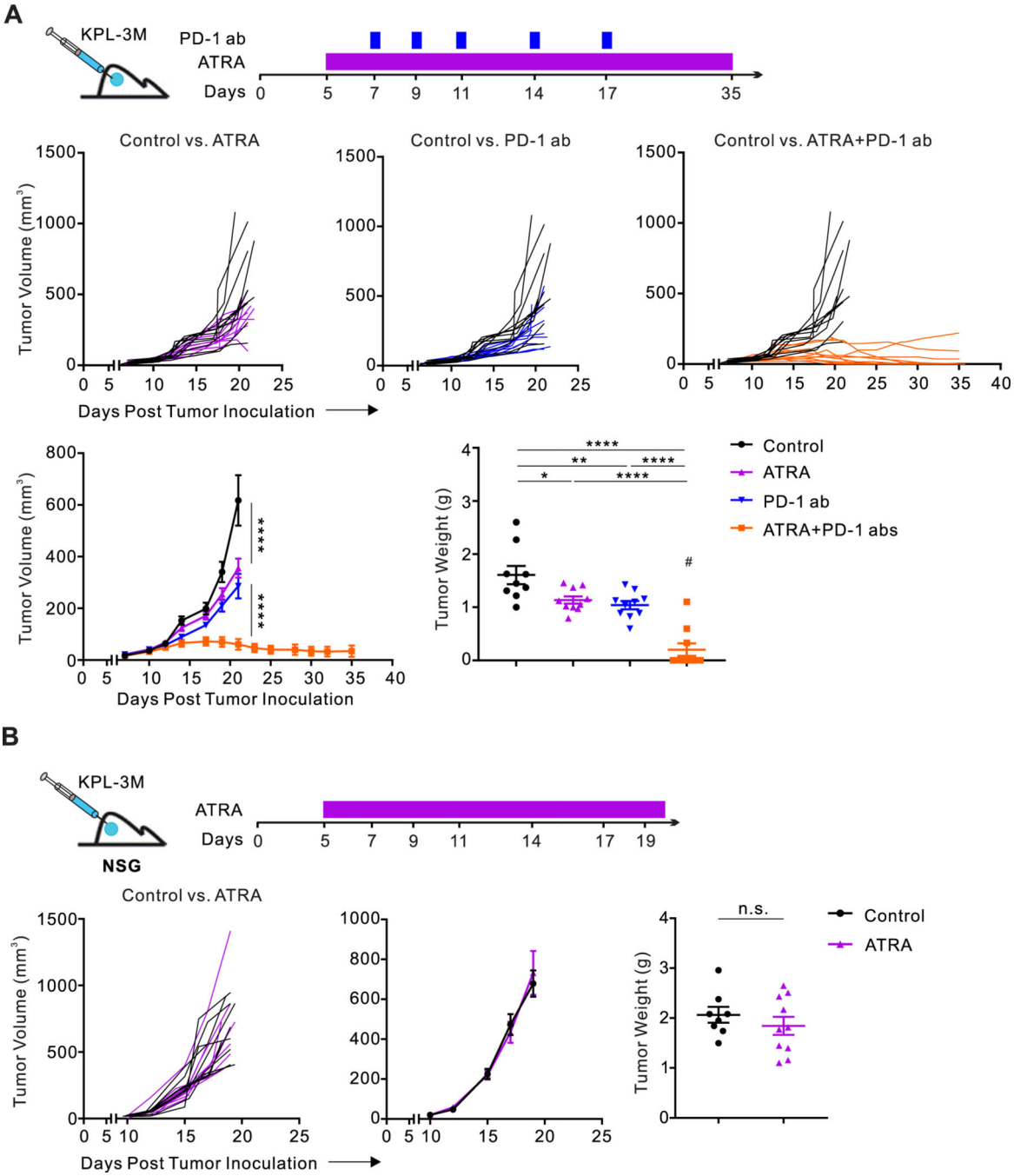

Figure 5. ATRA potentiates the efficacy of anti-PD-1 therapy in *Lkb1*-mutant NSCLC.

A) After subcutaneous inoculation of FVB mice with 1.5×10^5 KPL-3M cells, ATRA (purple box) treatment was started on day 5 and given daily until the end of the study, and anti-PD-1 (blue box) therapy was given in five doses as indicated. Growth curves and corresponding tumor weights at the time of euthanasia are presented. Results are representative of at least three biological replicates of 6–10 mice per group. **B**) 1.5×10^5 KPL-3M cells were injected subcutaneously on the flank of NSG mice, and mice were treated daily with either vehicle control or ATRA. * $P<0.05$; **, $P< 0.01$; ****, $P< 0.0001$.

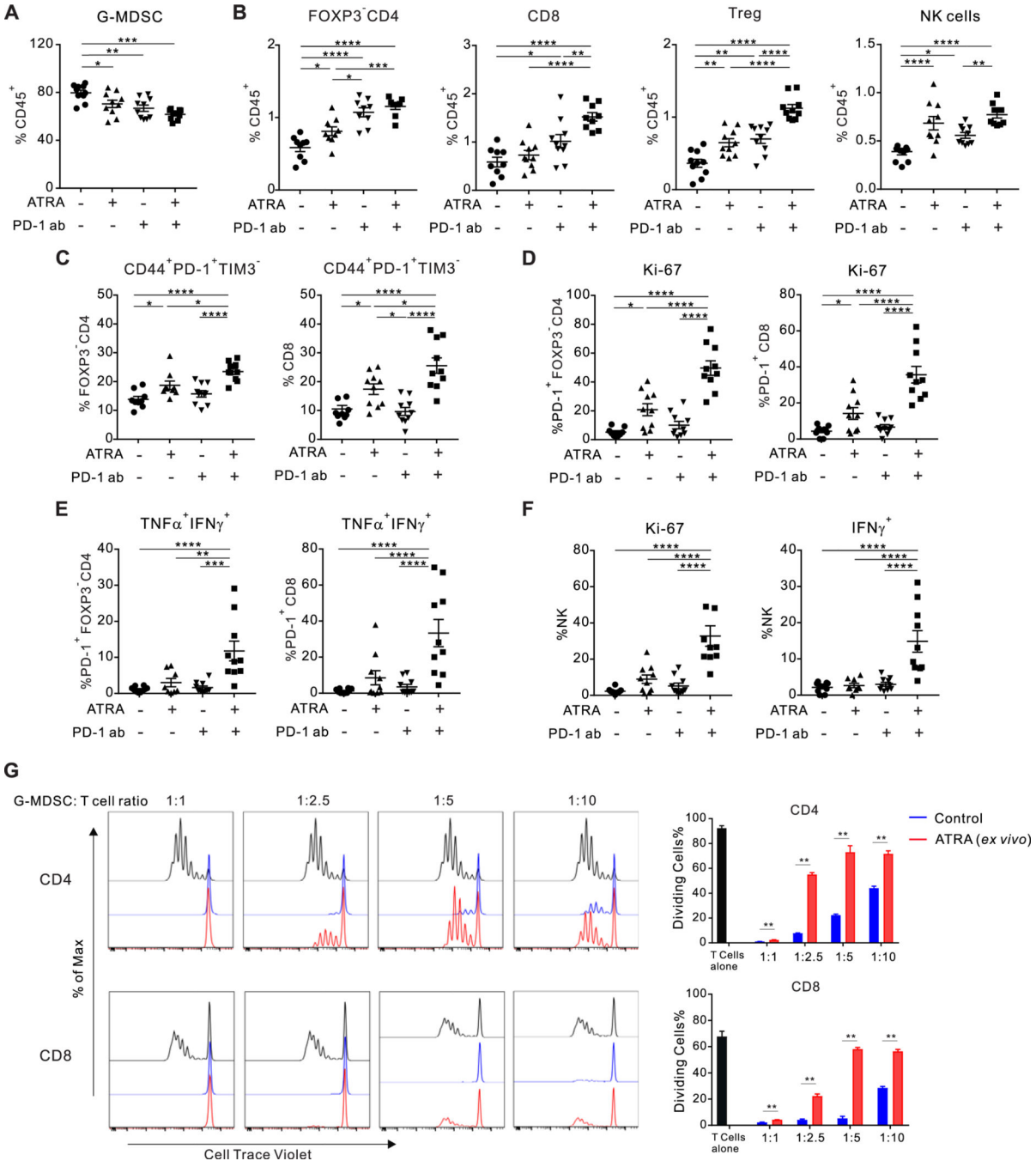

Figure 6. ATRA therapy suppresses the proliferation and function of G-MDSCs, and leads to enhanced T cell infiltration, proliferation and activation in the TME of LKB1-deficient NSCLC.

After subcutaneous inoculation of FVB mice with 1.5×10^5 KPL-3M cells, daily ATRA treatment was started on day 5, and anti-PD-1 therapy was given on days 7, 9, 11, and 14. Mice were euthanized on day 17 for immunophenotyping by flow cytometry. **A**) The abundance of G-MDSC in the TME. **B**) The abundance of FOXP$^-$CD4, CD8, Treg, and NK cells in the TME. **C**) The abundance of CD44$^+$PD-1$^+$ TILs. **D**) Percentage of Ki-67 positive cells in PD-1$^+$FOXP3$^-$CD4, and PD-1$^+$CD8 TILs. **E**) Secretion of TNFα and IFNγ

from PD-1^{+}FOXP3^{-}CD4, and PD-1^{+}CD8 TILs. **F**) Proliferation and IFNγ secretion of tumor-infiltrating NK cells. Treatment is indicated at the bottom of each graph. Results are representative of at least three biological replicates of 6–10 mice per group. **G**) After subcutaneous inoculation of FVB mice with 1.5×10^{5} KPL-3M cells, daily treatment with ATRA (red) or vehicle control (blue) was started on day 5. Tumor-infiltrating G-MDSCs were flow-sorted and co-cultured with CellTrace Violet-labeled murine T cells from naïve spleens at indicated ratios, and stimulated with IL-2 and αCD3/αCD28 beads. Flow histograms and quantification of T cell proliferation are presented. * $P<0.05$; **, $P< 0.01$; ***, $P<0.001$; ****, $P< 0.0001$.

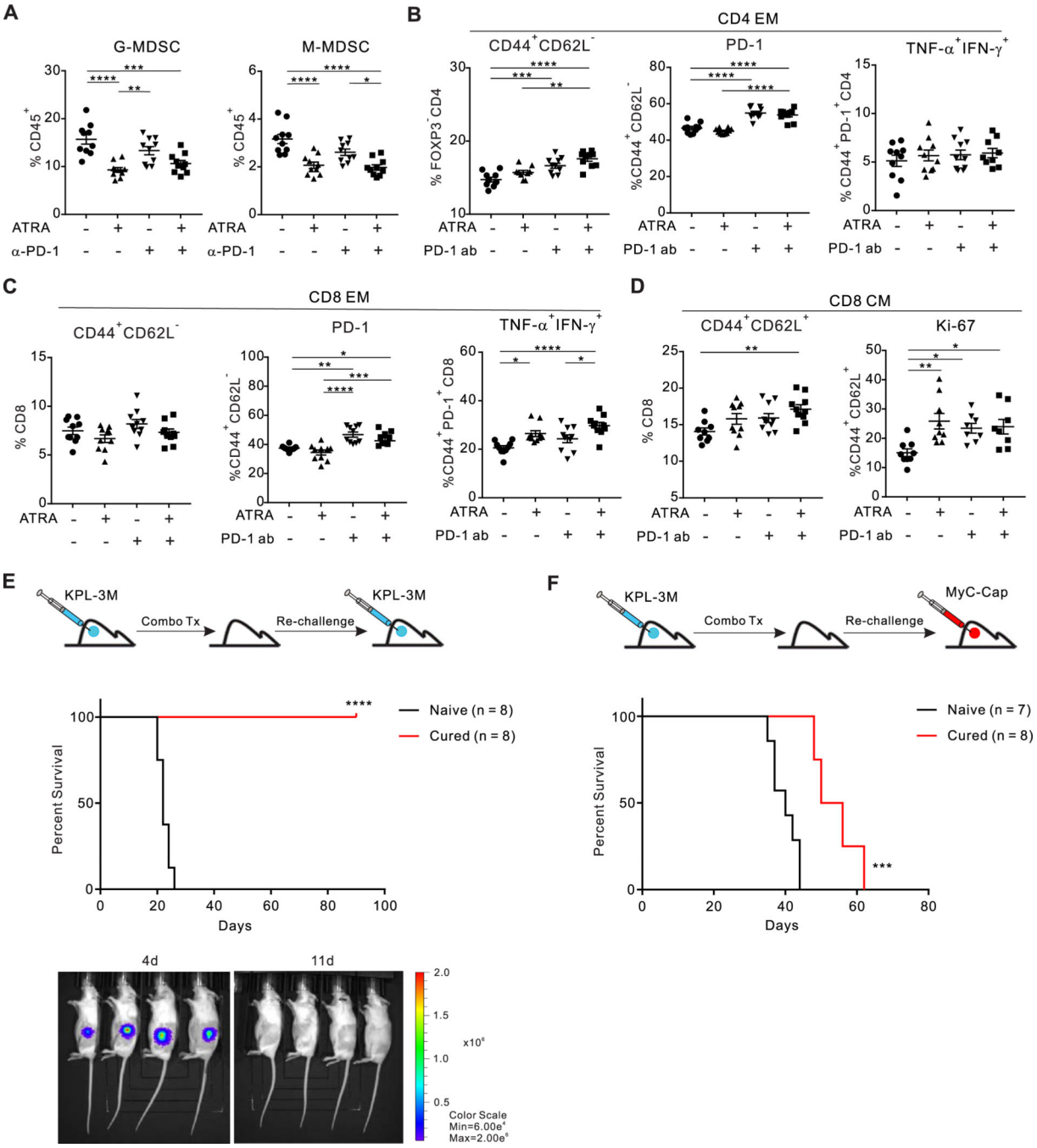

Figure 7. Combination therapy with ATRA and anti-PD-1 induces systemic tumor-specific immune memory.

Immunophenotyping of murine spleens from the same experiment as Fig. 6. **A**) The abundance of G-MDSC and M-MDSC in spleen. **B**) Percentage of $CD44^{+}CD62L^{-}$ EM cells within $FOXP3^{-}CD4$ T cells (left) and the percentage of $PD\text{-}1^{+}$ cells within $FOXP3^{-}CD4$ EM T cells (middle) in the spleen. Secretion of TNFα and IFNγ from $CD44^{+}PD\text{-}1^{+}FOXP3^{-}CD4$ T cells in the spleen (right). **C**) Percentage of EM cells within CD8 T cells (left) and the percentage of $PD\text{-}1^{+}$ cells within CD8 EM T cells (middle) in the spleen. Secretion of

TNFα and IFNγ from $CD44^+PD\text{-}1^+CD8$ T cells in the spleen (right). **D**) Percentage of $CD44^+CD62L^+$ CM CD8 T cells and their proliferation rates indicated by Ki-67 staining. **E**) Mice that had rejected KPL-3M tumors following combination therapy with ATRA and anti-PD1 were inoculated with KPL-3M (2×10^5 cells) and tumor growth was assessed with bioluminescence imaging on day 4 (4d) and day 11 (11d). Naïve mice served as control. Survival plot is presented. Results are representative of at least three biological replicates of 6–10 mice per group. **F**) Mice that had rejected KPL-3M tumors following combination therapy with ATRA and anti-PD1 were inoculated with MyC-CaP (2×10^6 cells). Naïve mice served as control. Survival plot is presented. Results are representative of at least two biological replicates of 6–10 mice per group. * $P<0.05$; **, $P< 0.01$; ***, $P<0.001$; ****, $P< 0.0001$.